# Dynamics and Stability Analysis of a Tethered Unmanned Rotorcraft

Alexander Donkels*

*DLR Institute of Flight Systems, Braunschweig, 38108, Germany*
*University of Maryland, College Park, Maryland, 20742, USA*

Johann C. Dauer[†]

*DLR Institute of Flight Systems, Braunschweig, 38108, Germany*

Derek A. Paley[‡]

*University of Maryland, College Park, Maryland, 20742, USA*

**Naval aviators use tethers to assist rotorcraft during ship board landing because of the ability to increase robustness against wind turbulence and to center the rotorcraft on the landing spot. Autonomous tethered landing with unmanned rotorcraft and automatic winch device for applying the tether force requires the knowledge of how the tether force impacts the wind affected dynamics of the rotorcraft. To this day, the influences of applied tether force and wind velocity on robustness and stability of the rotorcraft have been little explored. In this paper, we present an analysis of the dynamics and stability of a nonlinear model of a small-scale tethered rotorcraft. We develop a simplified model of a rotorcraft's longitudinal dynamics and vary model parameters including tether force, trim conditions, and the horizontal wind in order to study the interdependence of those parameters and their impact on the model's equilibrium points and stability. This is a preliminary step towards design of an automatic control of an unmanned rotorcraft capable of autonomous tethered landing and development of tether force control laws for the winch device.**

## Nomenclature

| | | |
|---|---|---|
| $a$ | = | Longitudinal flapping angle |
| $A$ | = | Dynamic matrix |
| $b$ | = | Lateral flapping angle |
| $B$ | = | Input matrix |
| $I_{yy}$ | = | Moment of inertia |
| $m$ | = | Mass |
| $M$ | = | Torque around pitch axis |
| $M_{lon}$ | = | Pitch gain |
| $M_0$ | = | Static pitching moment |
| $q$ | = | Pitch velocity |
| $R\Omega$ | = | Rotor tip velocity |
| $\mathbf{r}_{i/j}$ | = | Radius vector of point $i$ with respect to origin $j$ in body frame |
| $T$ | = | Tether force |
| $u, v, w$ | = | Linear velocities in body frame |
| $\mathbf{u}$ | = | Input vector |
| $V_W$ | = | Horizontal wind velocity |

---

*Research Scientist, Department of Unmanned Aircraft Systems, DLR Institute of Flight Systems, Lilienthalplatz 7, 38108 Braunschweig, Germany, alexander.donkels@dlr.de .

[†]Head of Department of Unmanned Aircraft Systems, DLR Institute of Flight Systems, Lilienthalplatz 7, 38108 Braunschweig, Germany, johann.dauer@dlr.de .

[‡]Willis H. Young Jr. Professor of Aerospace Engineering Education, Department of Aerospace Engineering and Institute for Systems Research, University of Maryland, College Park, MD 20742. AIAA Senior Member.

| | | |
|---|---|---|
| $x$ | = | Horizontal position |
| $\mathbf{x}$ | = | State vector |
| $X$ | = | Horizontal force in body frame |
| $X_u$ | = | Horizontal fuselage aerodynamic drag scaler |
| $X_{rd}$ | = | Horizontal rotor drag |
| $z$ | = | Vertical position |
| $Z$ | = | Vertical force in body frame |
| $Z_0$ | = | Static rotor thrust |
| $Z_{col}$ | = | Collective gain |
| $Z_{rd}$ | = | Vertical rotor drag derivative |
| $Z_w$ | = | Vertical fuselage aerodynamic drag scaler |
| $\alpha, \beta$ | = | Tether angle |
| $\delta_{lat}, \delta_{lon}, \delta_{ped}, \delta_{col}$ | = | Roll, pitch, yaw, and thrust inputs |
| $\theta$ | = | Pitch angle |
| $\lambda$ | = | Inflow ratio |
| $\mu$ | = | Advance ratio |
| $\phi$ | = | Roll angle |

# I. Introduction

For many decades, the tethered ship board landing method assists helicopter pilots land on moving ship decks in severe weather conditions. Crucial to the use of unmanned rotorcraft for ship board operations is the ability to safely and reliably deploy and recover the rotorcraft in even severe weather conditions. Automation of tether guided recovery provides a way to actively increase system robustness against weather and ship wake turbulence through the tether force and to center the rotorcraft on the landing spot. The tether may also serve as a reliable sensor source for relative navigation to the ship deck.



(a) DLR unmanned demonstrator superARTIS lands tether-guided on a ship deck.

(b) DLR meARTIS demonstrator on the left, intelligent winch prototype on the right.

**Fig. 1  Demonstrators for tethered ship board landing**

The purpose of the tether in ship board landing is to support the rotorcraft in controlling its position and attitude relative to the ship deck to ensure proper alignment for the landing. The winch device responsible for controlling the tether force introduces new degrees of freedom to the dynamics. Control design for the winch force requires understanding of how the tether force affects the ability to maintain a desired alignment with the ship. The tether also introduces new constraints to the rotorcraft dynamics, which result in interdependence of tether length, tether force, wind, and trim condition for a desired equilibrium. These interdependences have been observed but not followed up in previous publications. Especially the impact of parameters other than the tether length need to be investigated. Thus, we create a simplified nonlinear model of a tethered rotorcraft. We use this model to study the sensitivity of the model's equilibrium points to tether force, static horizontal wind, and trim condition in terms of their number and position for different ratios of force to thrust. We then study the eigenvalues of the model to evaluate the tether's impact on the

model's stability. We use the methods of sensitivity and stability analysis, based on the location of eigenvalues, to study through a simple model whether the tether causes the model to bifurcate, i.e. unstable eigenvalues become stable or the number of equilibria changes.

The German Aerospace Center (DLR) conducts research on tethered rotorcraft with the technology demonstrators shown in Figure 1. superARTIS is a turbine-driven helicopter with intermeshing blades, and with 85 kg maximum take-off mass, the largest member of the family of Autonomous Research Testbeds for Intelligent Systems (ARTIS). meARTIS is a 12 kg, fully electric helicopter with tail rotor and Bell-Hiller stabilizer. meARTIS is based on its predecessor midiARTIS, a helicopter with the same rotor configuration, but a methanol combustion engine, for which an identified model, created by Lorenz and Chowdhary, is available in [1]. In [2], Schuchardt et al. present how a newly developed portable winching device, shown in Fig. 1b, is able to establish a tethered connection to a ship deck for takeoff and landing. The concept as well as the winch have been tested in flight tests on a ship deck in the harbor of Warnemünde, Germany. [2]

Tethered rotorcraft have been in the focus of various research communities and over several periods of time. Research within the rotorcraft community in the 1960s and 1970s elaborated whether then state-of-the-art control methods are able to stabilize a tethered rotorcraft. Kaufman and Schultz investigated [3] the hovering behavior of a tethered helicopter using a linearized model extended by a rigid tether*. Kaufman and Schultz found the tether produces an infinite number of steady hovering states and they identified two additional modes of longitudinal motion, that are introduced by the degrees of freedom of the tether: the stable pitching mode and the unstable pendulum mode. The characteristics of both modes are influenced by the tether length and the unstable pendulum mode can be stabilized by a controller.

Research efforts within the robotics community starting in the 2000s focused on design and proof of stability of control designs for the tethered rotorcraft. Oh et al. discovered in [4] that the tether allows control of the rotorcraft's attitude through linear motion and accordingly designed a cascaded controller with the ability to switch between the control objectives of velocity and attitude control. Ahmed et al. used backstepping control [5] and Sandino et al. designed a feed-forward extension to an existing controller [6] to counteract the observed coupling of linear and rotational motion. Sandino et al. also proposed the existence of an optimal ratio of tether force and the rotorcraft's mass to maximize robustness against wind turbulence. Note, Ahmed et al. and Sandino et al. used the tether force as an input variable to their flight controller.

In the context of the work of Sandino et al. in [7], Alarcón et al. showed in [8] a concept for position estimation using a cable link to replace a satellite navigation system as source for helicopter position control. Alarcón demonstrated the functionality of this method in flight experiments.[8] This work does not focus on the change of dynamics through the tether, but demonstrates that tethered autonomous vehicles can be precisely controlled to perform landings on moving platforms.

This paper presents the first steps on evaluation of the influence of the tether force, tether length, horizontal wind, and control inputs on a small-scale tethered rotorcraft. We also evaluate how the tether constraints impact the interdependence of these variables. We design a nonlinear model of the tethered rotorcraft with reduced complexity. In order to reduce the complexity, we consider only longitudinal motion. We also replace the complex dynamics of the main rotor with a simple thrust and drag model for the benefit of reducing the number of parameters. We evaluate the equilibrium points and eigenvalues of the system as a function of tether force, tether length, wind velocity, and trim inputs. Further research could expand upon the knowledge for designing control laws for winch and rotorcraft to stabilize the system while maximizing the benefits of the tether.

The contributions of this paper are (1) the construction of a nonlinear state space model with tether and wind influence and (2) the evaluation of the dependence of equilibrium points and eigenvalues of the linearized model to changes of tether force, tether length, trim conditions, and wind velocity. The results can be used to identify setpoints for tether force and helicopter thrust to alter the helicopter's dynamics in a beneficial way and to analyze the dynamic's dependency on the tether length, which decreases during the landing maneuver. The consideration of wind velocity increases the robustness of the results regardless of different weather conditions.

---

*Rigid tether refers to an applied force of constant value and its direction is defined by the straight line between the anchor points on the rotorcraft and the winch.

Section II discusses modelling methods for small rotorcraft to motivate the use of a nonlinear model to represent the tethered system. The basic assumptions for reduction of model complexity and state space form of the nonlinear model is elaborated in Section III. Section IV identifies parameters relevant for equilibrium and dynamical stability of the model. The paper concludes with a summary and an outlook on ongoing and future research in Section V.

## II. Background

This section provides background on existing models for small-scale rotorcraft. The first subsection focuses on nonlinear models and the second subsection describes linear modelling approaches through linearization or model identification.

### A. Nonlinear Modelling of Small Rotorcraft

Small rotorcraft typically possess high maneuvering capabilities and, relatively to their dimension, large flight envelope as compared to large rotorcraft. A broad part of the flight envelope can be accurately represented by nonlinear models. A typical use of nonlinear models is for simulation and controller synthesis for acrobatic flights [9]. Other examples for elaboration of nonlinear models for comparable purposes are [10] and [11], where models for small helicopters with a Bell-Hiller stabilizer are developed.

Nonlinear models use first principle mechanics to include all essential physical influences responsible for rotorcraft motion. A primary focus of the modelling efforts is the main rotor dynamics. The main rotor dynamics are usually represented by aerodynamical models to determine rotor thrust, drag, and moments based on rotor inflow and blade motion (bending and torsion). Structural models of the blades describe the blade motion as a result of aerodynamic loads, structural loads, and motion of the swashplate. The resulting models have parameters that cannot be directly measured and need to be approximated. Also, the model's state representation may contain some unobservable states like the flapping angles, which describe the blade motion, or the rotor inflow velocities. A drawback of the rotor inflow is that it needs to be approximated iteratively while solving the rotor dynamics, which increases computational effort. Accurate representation of blade flapping angles requires solving second-order differential equations.[9]

Methods to reduce model complexity are linearization of the rotor dynamics or reduction of flapping angle dynamics to first-order differential equations. Usually, flight experiments generate data to approximate the unknown parameters. We reduce the model complexity even further as we want to study whether sensitivity and stability analysis lead to new insights of the tether's influence on the model. The alternative to a nonlinear model is to use flight experiments to identify parameters of a linear model, which is described in the next subsection.

### B. Linear Modelling of Small Rotorcraft

Linear models of small scale rotorcraft can be obtained from dynamical identification as in [12] or lineariziation of an existing nonlinear model around an equilibrium [11]. Dynamical identification similar to [12] has been conducted for midiARTIS, a version of meARTIS with a combustion engine [1]. The linear model for midiARTIS uses the general state space system form

$$\dot{\mathbf{x}} = \mathbf{A}\mathbf{x} + \mathbf{B}\mathbf{u} \tag{1}$$

with state vector $\mathbf{x} = (u\ v\ w\ p\ q\ r\ a\ b\ \theta\ \phi)^T$ and input vector $\mathbf{u} = (\delta_{lat}\ \delta_{lon}\ \delta_{ped}\ \delta_{col})^T$. The variables $a$ and $b$ represent the flapping angles for the longitudinal and lateral motion, respectively. The inputs $\delta_{lat}$, $\delta_{lon}$, and $\delta_{col}$ refer to motions of the main rotor swashplate to control roll, pitch, and vertical motion, respectively. The tail rotor input $\delta_{ped}$ changes the tail rotor thrust to control yaw motion. We will adapt the notation for input and state variables of the linear model to the description of our nonlinear model in Section III.

Linear models are widely used for flight controller synthesis in simulations and for model-based control. Based on good flight test data, identification methods can produce linear models of high dynamical accuracy and high bandwidth and can be used to improve nonlinear models [12]. These benefits come for the price of the model being only valid in some close proximity to the equilibrium point the model was identified or linearized at, which limits investigations with the model to a very small part of the flight envelope.

In this work, the flight envelope represented by the model should be as large as possible, which favors development of a nonlinear model. Also, the nonlinear model is most suitable for representing the nonlinear influence of the tether, because of the existence of multiple equilibrium points.

## III. Nonlinear Dynamics of a Tethered Rotorcraft

This section presents the modelling approach for a tethered rotorcraft. First, we present mathematical formulations for the kinematics and for acting forces and moments and introduce methods to simplify the dynamics where needed. Then, we formulate a state space model representation of the system and introduce a transformation to express the rotorcraft position in polar coordinates. In a last step, we present an estimate of model parameters.

### A. Modelling Forces and Moments

The kinematics of the tethered rotorcraft model are expressed in the body frame $\mathcal{B}$ with respect to an inertial frame $\mathcal{I}$. For reduction of complexity, only the sideslip-free longitudinal motion with no roll angle in two dimensions is defined. The Eqs. 2 to 7 express the 2-dimensional kinematics for the position of the center of mass $G$ as $x$ and $z$, the linear velocity as $u$ and $w$, the pitch angle $\theta$, and pitch velocity $q$. The mass of the rotorcraft is $m$ and its moment of inertia around the pitch axis is $I_{yy}$. We have

$$u = \frac{d}{dt}x = \dot{x} \tag{2}$$

$$w = \frac{d}{dt}z = \dot{z} \tag{3}$$

$$X = X_f + X_{mr} + X_g + X_t = m\,\dot{u} + m\,q\,w \tag{4}$$

$$Z = Z_f + Z_{mr} + Z_g + Z_t = m\dot{w} - m\,q\,u \tag{5}$$

$$q = \frac{d}{dt}\theta = \dot{\theta} \tag{6}$$

$$M = M_f + M_{mr} + M_t = I_{yy}\,\dot{q}\,. \tag{7}$$

The acting forces on the body are the aerodynamic drag on the fuselage $f$, main rotor $mr$ drag, thrust, and pitching moment, the weight $g$, and the tether force $t$. Reference frames, forces, and moments are depicted in Fig. 2. The origin of the inertia frame is denoted $O$. Main rotor forces are assumed to act at point $R$, defined by the intersection of the rotor disc plane and rotor mast. The aerodynamic forces acting on the fuselage attack at the neutral point $N$. The tether forces attack at the anchor point $A$. The position $\mathbf{r}$ of these points are defined as follows:

$$\mathbf{r}_{G/O} = \begin{bmatrix} x \\ z \end{bmatrix}_{\mathcal{B}}, \quad \mathbf{r}_{A/G} = \begin{bmatrix} x_{A/G} \\ z_{A/G} \end{bmatrix}_{\mathcal{B}}, \quad \mathbf{r}_{N/G} = \begin{bmatrix} x_{N/G} \\ z_{N/G} \end{bmatrix}_{\mathcal{B}}, \quad \mathbf{r}_{R/G} = \begin{bmatrix} x_{R/G} \\ z_{R/G} \end{bmatrix}_{\mathcal{B}}. \tag{8}$$

The aerodynamic forces are simplified and modelled under the assumption of constant air density $\rho$, constant drag coefficient $C_D$, and constant reference surface $S$. The moment $M_{f,0}$ around the neutral point $N$ is independent of the angle of attack, but depends on the flow velocity. As this work focuses on the model dynamics in and around the equilibrium point, non-essential change of the flow velocity can be assumed. Thus, assume the moment $M_{f,0}$ is constant and compensated by the trim moment. Consequentially, $M_{f,0}$ is not used in any of the following equations for the fuselage. The used drag coefficient is independent of the direction and velocity of the air flow. Assume that the projected surface and drag coefficient in direction of the body axes $x$ and $z$ are different. The subscripts $x, f$ and $z, f$ denote the different values for $C_D$ and $S$ according to the body axis. For the fuselage, the aerodynamic forces acting at point $N$ and their torque $M_f$ with respect to $G$ are

$$\begin{bmatrix} X_f \\ Z_f \\ M_f \end{bmatrix}_{\mathcal{B}} = \begin{bmatrix} \underbrace{-\frac{\rho}{2}C_{D,x,f}S_{f,x}\,(u + V_W\cos\theta)\,|u + V_W\cos\theta|}_{=X_u} \\ \underbrace{-\frac{\rho}{2}C_{D,z,f}S_{f,z}\,(w + V_W\sin\theta)\,|w + V_W\sin\theta|}_{=Z_w} \\ z_{N/G}X_f - x_{N/G}Z_f + M_{f,0} \end{bmatrix}_{\mathcal{B}}. \tag{9}$$

For transparency, the constant parameters $\rho$, $C_D$, and $S$ are aggregated to the parameters $X_u$ and $Z_w$ for the $x$ and $z$ directions, respectively.

The rotor dynamics of the rotorcraft are simplified to avoid iterations for inflow approximation and solving for the blade flapping motion. Assume the thrust force $T_{mr}$ and pitching moment $M_{mr}$ are independently controllable and the rotor disc interaction with the flow is modelled by the drag force model introduced by Sun et al. in [13]. In the following, we describe the adaptation of Sun et al.'s model to our model.

The main rotor thrust $T_{mr}$ acts perpendicularly to the rotor frame and in the $z$-direction of the body frame. $T_{mr}$ consists of a static thrust $Z_0$ for trimming and the thrust input $\delta_{col}$ with linear gain $Z_{col}$. The perpendicular flow through the rotor $w + V_W \sin \theta$ changes the inflow ratio $\lambda$ through the rotor disc and causes a change of the rotor thrust. Thus, the rotor thrust linearly increases or decreases with the parameter $Z_{mr,\lambda}$ and change of inflow ratio $\Delta\lambda$:

$$\Delta\lambda = \frac{w + V_W \sin \theta}{R\Omega}, \tag{10}$$

where the term $R\Omega$ denotes the rotor tip velocity. The main rotor thrust $T_{mr}$ is

$$T_{mr} = (Z_0 + Z_{col}\,\delta_{col})\left(1 + \underbrace{Z_{mr,\lambda}\frac{w + V_W \sin \theta}{R\Omega}}_{=Z_{rd}(w + V_W \sin \theta)}\right). \tag{11}$$

The parameters $R\Omega$ and $Z_{mr,\lambda}$ are combined in the new parameter $Z_{rd}$. The tangential flow through the rotor $u + V_W \cos \theta$ causes a flapping angle $b$ between the the rotor disc and the body frame and a tilt of the rotor thrust $T_{mr}$. Assuming small angles for $a$, as also done in [9], leads to

$$\begin{bmatrix} X_{mr} \\ Z_{mr} \end{bmatrix}_{\mathcal{B}} = \begin{bmatrix} -T_{mr}\sin a \\ -T_{mr}\cos a \end{bmatrix}_{\mathcal{B}} \approx \begin{bmatrix} -T_{mr}a \\ -T_{mr} \end{bmatrix}_{\mathcal{B}}. \tag{12}$$

According to [13], the longitudinal flapping angle $a$ can be calculated using the advance ratio $\mu$ and a linear parameter $X_{mr,u}$

$$a = X_{mr,u}\mu = X_{mr,u}\frac{u + V_W \cos \theta}{R\Omega}. \tag{13}$$

The control of the main rotor pitching moment consists of a trim moment $M_0$, pitch input $\delta_{lon}$, and pitch input gain $M_{lon}$. Forces and moments of the main rotor are

$$\begin{bmatrix} X_{mr} \\ Z_{mr} \\ M_{mr} \end{bmatrix}_{\mathcal{B}} = \begin{bmatrix} \underbrace{-\dfrac{T_{mr}}{R\Omega}X_{mr,u}\,(u + V_W \cos \theta)}_{=T_{mr}X_{rd}} \\ -T_{mr} \\ z_{R/G}X_{mr} - x_{R/G}Z_{mr} + M_0 + M_{lon}\,\delta_{lon} \end{bmatrix}_{\mathcal{B}}. \tag{14}$$

For transparency, constant parameters are aggregated to $X_{rd}$ and $Z_{rd}$ for rotor forces in x and z direction, respectively. Forces and moments at and around $G$ are

$$\begin{bmatrix} X_g \\ Z_g \\ M_g \end{bmatrix}_{\mathcal{B}} = \begin{bmatrix} -m\,g\sin\theta \\ m\,g\cos\theta \\ 0 \end{bmatrix}_{\mathcal{B}}. \tag{15}$$

Neglecting tether dynamics, tether forces are modelled to be of constant force $T$. The direction of $T$ is defined by the direction of $\mathbf{r}_{O/A} = -\left(\mathbf{r}_{A/G} + \mathbf{r}_{G/O}\right)$.

$$\begin{bmatrix} X_t \\ Z_t \\ M_t \end{bmatrix}_{\mathcal{B}} = \begin{bmatrix} T\frac{r_{O/A,x}}{||r_{O/A}||_2} \\ T\frac{r_{O/A,z}}{||r_{O/A}||_2} \\ z_{A/G}X_t - x_{A/G}Z_t \end{bmatrix}_{\mathcal{B}} = \begin{bmatrix} -T\frac{x + x_{A/G}}{\sqrt{\left(x + x_{A/G}\right)^2 + \left(z + z_{A/G}\right)^2}} \\ -T\frac{z + z_{A/G}}{\sqrt{\left(x + x_{A/G}\right)^2 + \left(z + z_{A/G}\right)^2}} \\ z_{A/G}X_t - x_{A/G}Z_t \end{bmatrix}_{\mathcal{B}} \tag{16}$$
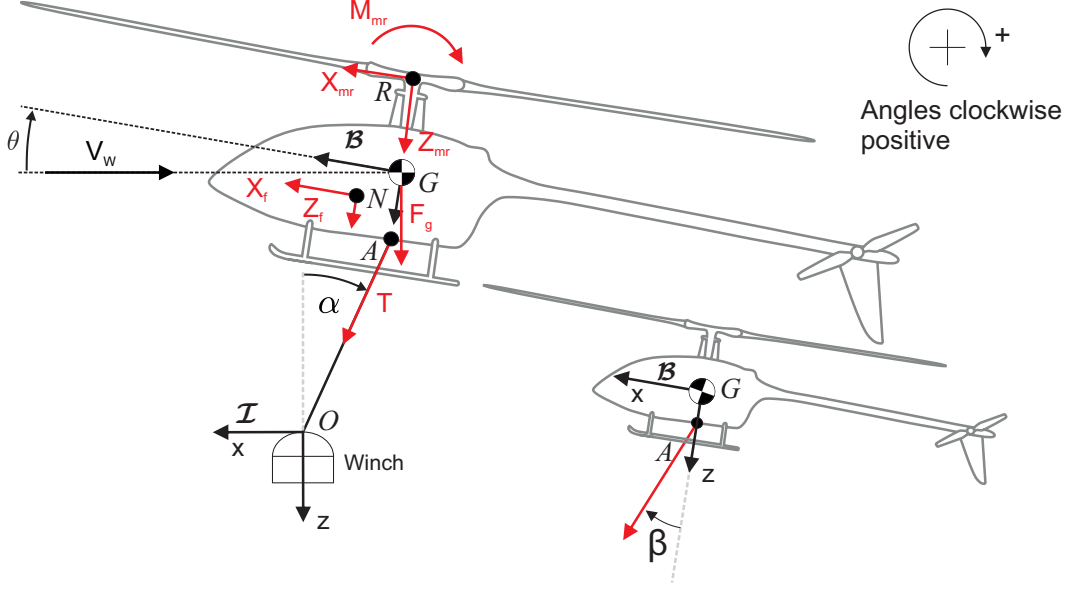
**Fig. 2  Forces and moments acting on the helicopter.**

## B. Equations of Motion

The combined dynamics and kinematics of the model yield a system of the form $\dot{\mathbf{x}} = \mathbf{f}(\mathbf{x}) + \mathbf{g}(\mathbf{x})\mathbf{u}$ with the state vector $\mathbf{x} = (x\ z\ u\ w\ \theta\ q)^T$ and the input vector $\mathbf{u} = (\delta_{lon}\ \delta_{col})^T$. The state space form of the model is

$$\dot{x} = u \tag{17}$$

$$\dot{z} = w \tag{18}$$

$$\dot{u} = -qw - g\sin\theta - \frac{X_u}{m}|u + V_W\cos\theta|(u + V_W\cos\theta) - \frac{T}{m}\frac{x + x_{A/G}}{\sqrt{(x + x_{A/G})^2 + (z + z_{A/G})^2}} - \dots$$

$$+ \frac{X_{rd}}{m}(u + V_W\cos\theta)(Z_0 + Z_{col}\,\delta_{col} + (Z_0 + Z_{col}\,\delta_{col})Z_{rd}(w + V_W\sin\theta)) \tag{19}$$

$$\dot{w} = qu + g\cos\theta - \frac{Z_w}{m}|w + V_W\sin\theta|(w + V_W\sin\theta) - \frac{T}{m}\frac{z + z_{A/G}}{\sqrt{(x + x_{A/G})^2 + (z + z_{A/G})^2}} - \dots$$

$$- Z_0 - Z_{col}\,\delta_{col} - (Z_0 + Z_{col}\,\delta_{col})Z_{rd}(w + V_W\sin\theta) \tag{20}$$

$$\dot{\theta} = q \tag{21}$$

$$\dot{q} = -\frac{T}{I_{yy}}\frac{x + x_{A/G}}{\sqrt{(x + x_{A/G})^2 + (z + z_{A/G})^2}}z_{A/G} + \frac{T}{I_{yy}}\frac{z + z_{A/G}}{\sqrt{(x + x_{A/G})^2 + (z + z_{A/G})^2}}x_{A/G} - \dots$$

$$- \frac{X_u}{I_{yy}}|u + V_W\cos\theta|(u + V_W\cos\theta)\,z_{N/G} + \dots$$

$$+ \frac{Z_w}{I_{yy}}|w + V_W\sin\theta|(w + V_W\sin\theta)\,x_{N/G} + \dots$$

$$- \frac{1}{I_{yy}}X_{rd}(u + V_W\cos\theta)(Z_0 + Z_{col}\,\delta_{col} + (Z_0 + Z_{col}\,\delta_{col})Z_{rd}(w + V_W\sin\theta))\,z_{R/G} + \dots$$

$$+ \frac{1}{I_{yy}}(Z_0 + Z_{col}\,\delta_{col} + (Z_0 + Z_{col}\,\delta_{col})Z_{rd}(w + V_W\sin\theta))\,x_{R/G} + \frac{M_{lon}}{I_{yy}}\delta_{lon} + M_0. \tag{22}$$

The Cartesian representation of the model's position by the variables $u$ and $w$ is commonly used and would serve rotorcraft pilots as a intuitive reference to steer the vehicle with respect to the winch position. However, the potentially important tether length $L$ would only be implicitly involved in the system model through the definition

$L = \sqrt{\left(x + x_{A/G}\right)^2 + \left(z + z_{A/G}\right)^2}$. A transformation from Cartesian coordinates $x, z$ to polar coordinates $L, \beta$, where $\beta$ denotes the tether force angle within $\mathcal{B}$, includes the tether length $L$ as a system variable. The rotation of $\beta$ is defined so that $\beta > 0$ refers to forward-acting tether force. The angle $\alpha$ defines the tether angle with respect to $\mathcal{I}$. Equation 23 defines the relation between $\alpha$ and $\beta$, which is based on the rotation from $\mathcal{I}$ to $\mathcal{B}$ through the pitch angle $\theta$, i.e.,

$$\alpha = \beta + \theta . \tag{23}$$

The following equations formulate the necessary transformation rule:

$$x = -L \sin \beta - x_{A/G} \tag{24}$$
$$z = -L \cos \beta - z_{A/G}. \tag{25}$$

The revised state space model is denoted with underscore $p$ and is described by $\dot{\mathbf{x}}_p = \mathbf{f}_p\left(\mathbf{x}_p\right) + \mathbf{g}_p\left(\mathbf{x}_p\right)\mathbf{u}$ with the state vector $\mathbf{x}_p = (L\ \beta\ u\ w\ \theta\ q)^T$ and the input vector $\mathbf{u} = (\delta_{lon}\ \delta_{col})^T$. The following equations represent the state space form of the transformed model:

$$\dot{L} = -u \sin \beta - w \cos \beta \tag{26}$$

$$\dot{\beta} = -\frac{u}{L} \cos \beta + \frac{w}{L} \sin \beta - q \tag{27}$$

$$\dot{u} = -qw - g \sin \theta - \frac{X_u}{m} |u + V_W \cos \theta| (u + V_W \cos \theta) + \frac{T}{m} \sin \beta - \dots$$
$$\frac{X_{rd}}{m} (u + V_W \cos \theta) (Z_0 + Z_{col}\, \delta_{col} + (Z_0 + Z_{col}\, \delta_{col}) Z_{rd} (w + V_W \sin \theta)) \tag{28}$$

$$\dot{w} = qu + g \cos \theta - \frac{Z_w}{m} |w + V_W \sin \theta| (w + V_W \sin \theta) + \frac{T}{m} \cos \beta - \dots$$
$$-Z_0 - Z_{col}\, \delta_{col} - (Z_0 + Z_{col}\, \delta_{col}) Z_{rd} (w + V_W \sin \theta) \tag{29}$$

$$\dot{\theta} = q \tag{30}$$

$$\dot{q} = \frac{T}{I_{yy}} \sin \beta\, z_{A/G} - \frac{T}{I_{yy}} \cos \beta\, x_{A/G} - \dots$$
$$-\frac{X_u}{I_{yy}} |u + V_W \cos \theta| (u + V_W \cos \theta)\, z_{N/G} + \dots$$
$$+\frac{Z_w}{I_{yy}} |w + V_W \sin \theta| (w + V_W \sin \theta)\, x_{N/G} + \dots$$
$$-\frac{1}{I_{yy}} X_{rd} (u + V_W \cos \theta) (Z_0 + Z_{col}\, \delta_{col} + (Z_0 + Z_{col}\, \delta_{col}) Z_{rd} (w + V_W \sin \theta))\, z_{R/G} + \dots$$
$$+\frac{1}{I_{yy}} (Z_0 + Z_{col}\, \delta_{col} + (Z_0 + Z_{col}\, \delta_{col}) Z_{rd} (w + V_W \sin \theta))\, x_{R/G} + \frac{M_{lon}}{I_{yy}} \delta_{lon} + M_0. \tag{31}$$

## C. Model parameters

The choice of adequate parameter values is crucial to achieve comparable behavior of the model to the real vehicle. Some parameters of the nonlinear model can be determined by simple measurements of the meARTIS rotorcraft or are available in literature. Examples are the vehicle's mass $m$ and the gravitational acceleration $g$. Other parameters, like the position of the fuselage's neutral point $N$ or the drag coefficients of rotor and fuselage cannot be easily determined. The following paragraph describes a simple method to assume values for the unknown parameters by comparison of the linearized model derivatives of the nonlinear model in hover with those derivatives of the identified model. This allows a good guess for the unknown parameters and well comparable model behavior around the hover condition.

System identification of the midiARTIS rotorcraft created a linear state space model for the hovering condition which is available in [1]. The longitudinal motion of the linearized system is described below, where $\mathbf{A}_{lon}$ and $\mathbf{B}_{lon}$ denote longitudinal dynamics and input gains, respectively. We have

$$\dot{\mathbf{x}} = \mathbf{A}_{lon}\mathbf{x} + \mathbf{B}_{lon}\mathbf{u} . \tag{32}$$

The linearization of the nonlinear model defined by Eqs. 26 to 31 around the hovering condition without wind and without tether force makes it possible to compare the derivatives of both systems for the longitudinal motion. The midiARTIS model was identified without any tether connection and its dynamics do not depend on the position. Thus, the derviatives for the positon are not available and only the derivatives for $u$, $w$, $\theta$, and $q$ can be compared. Consequently, The dimension of the matrix $A_{lon}$ for the comparison reduces to $4 \times 4$. We chose the parameters of the nonlinear system by hand to fit the derivatives of available experimental data of midiARTIS [1]. Equation 33 yields the dynamics of the linearized nonlinear system.

$$
\mathbf{A}_{lon}\mathbf{x} \quad = \quad
\begin{pmatrix}
-0.0589 & 0 & -9.81 & 0 \\
0 & -0.4905 & 0 & 0 \\
0 & 0 & 0 & 1.0 \\
-0.1483 & 0 & 0 & 0
\end{pmatrix}
\begin{pmatrix}
u \\
w \\
\theta \\
q
\end{pmatrix}
\tag{33}
$$

Table 1 in the Appendix lists the parameters for the nonlinear model. Some of the model parameters are varied in the following sections so that a range of values is given instead of one fixed value.

## IV. Stability Analysis of the Open-Loop Dynamics

This section formulates the equations defining equilibrium states and identifies parameters that have an influence on either the location of the equilibrium or the eigenvalues of the linearized system around the equilibrium. We vary the identified parameters and plot the results.

### A. Location of Equilibrium Points

To identify the equilibrium points of the system, set the left-hand side of Eqs. 26 to 31 can be set to zero. The inputs $\delta_{lon}$ and $\delta_{col}$ are set to zero, so that equilibrium is maintained by the static inputs $Z_0$ and $M_0$ (trimmed condition). From Eq. 30 follows that the pitch velocity in equilibrium is $q^* = 0$ and, from Eqs. 26 and 27, it follows that $u^* = 0$ and $w^* = 0$. The variables $u^* = 0$, $w^* = 0$, and $q^* = 0$ plugged into the remaining Eqs. 28, 29, and 31 yield:

$$
0 \quad = \quad -g \sin \theta^* - \frac{X_u}{m} V_W^2 \cos^2 \theta^* + \frac{T}{m} \sin \beta^* - \frac{X_{rd}}{m} Z_0 V_W \cos \theta^* \left(1 + Z_{rd} V_W \sin \theta^*\right)
\tag{34}
$$

$$
0 \quad = \quad g \cos \theta^* - \frac{Z_w}{m} \operatorname{sgn}\left(\theta^*\right) V_W^2 \sin^2 \theta^* + \frac{T}{m} \cos \beta^* - \frac{Z_0}{m} - \frac{Z_0}{m} V_W \sin \theta^*
\tag{35}
$$

$$
0 \quad = \quad \frac{T}{I_{yy}} \sin \beta^* z_{A/G} - \frac{T}{I_{yy}} \cos \beta^* x_{A/G} - \frac{X_u}{I_{yy}} V_W^2 \cos^2 \theta^* z_{N/G} + \ldots
$$
$$
+ \frac{Z_w}{I_{yy}} \operatorname{sgn}\left(\theta^*\right) V_W^2 \sin^2 \theta^* x_{N/G} + M_0 - \ldots
$$
$$
- \frac{Z_0}{I_{yy}} X_{rd} \left(V_W \cos \theta^*\right) Z_0 \left(1 + Z_{rd} V_W \sin \theta^*\right) z_{R/G} + \frac{Z_0}{I_{yy}} \left(1 + Z_{rd} V_W \sin \theta^*\right) x_{R/G}.
\tag{36}
$$

The tether length $L$ is not present in Eqs. 34 to 36. Thus, we can neglect $L$ when searching for the existence of equilibrium points. Also, we can choose $L$ independently from the other state variables and parameters. This is one of the advantages of transforming into polar coordinates. Note, the tether length still has an influence on the dynamics and must be included when investigating the stability of the equilibrium points.

Equations 34, 35, and 36 have only two unknowns, the tether angle $\beta^*$ and pitch angle $\theta^*$, which implies the system is overdetermined. Also, the static pitching moment $M_0$ is only present in the last of the equations. This means that the precise choice of $M_0$ decides whether the solutions to Eqs. 34 and 35 produce an equilibrium or not. Thus, the static pitching moment $M_0$ cannot be independently chosen from the state variables and other parameters and thus will no longer be considered for sensitivity analysis.

The remaining model parameters of interest are the tether force $T$, the static thrust $Z_0$ to trim the model, and wind velocity $V_W$. We examine the influence of these parameters on the location and existence of equilibrium points. In the following diagrams, we hold the trim $Z_0$ and wind $V_W$ constant, while varying the force $T$. This approach evaluates the system dynamics from the perspective of the winch, which controls the tether force. A different approach would be to

vary the thrust $Z_0$, which would give the perspective of the flight controller. We are planning to add this perspective in ongoing and future work.

Figures 3a and 3b show solutions for $\beta^*$, $\theta^*$, and their aggregate $\alpha^*$ for an example choice of wind velocity $V_W = 4$ m/s and a relatively low static thrust $Z_0 = 108$ N (a) and high static thrust $Z_0 = 180$ N (b), while the tether force $T$ is varied. The necessary static pitching moment $M_0$ for both cases is shown in Figs. 3c and 3d.



(a) Static thrust $Z_0 = 108$ N, wind velocity $V_W = 4$ m/s



(b) Static thrust $Z_0 = 180$ N, wind velocity $V_W = 4$ m/s



(c) Static pitching moment for $Z_0 = 108$ N and $V_W = 4$ m/s case



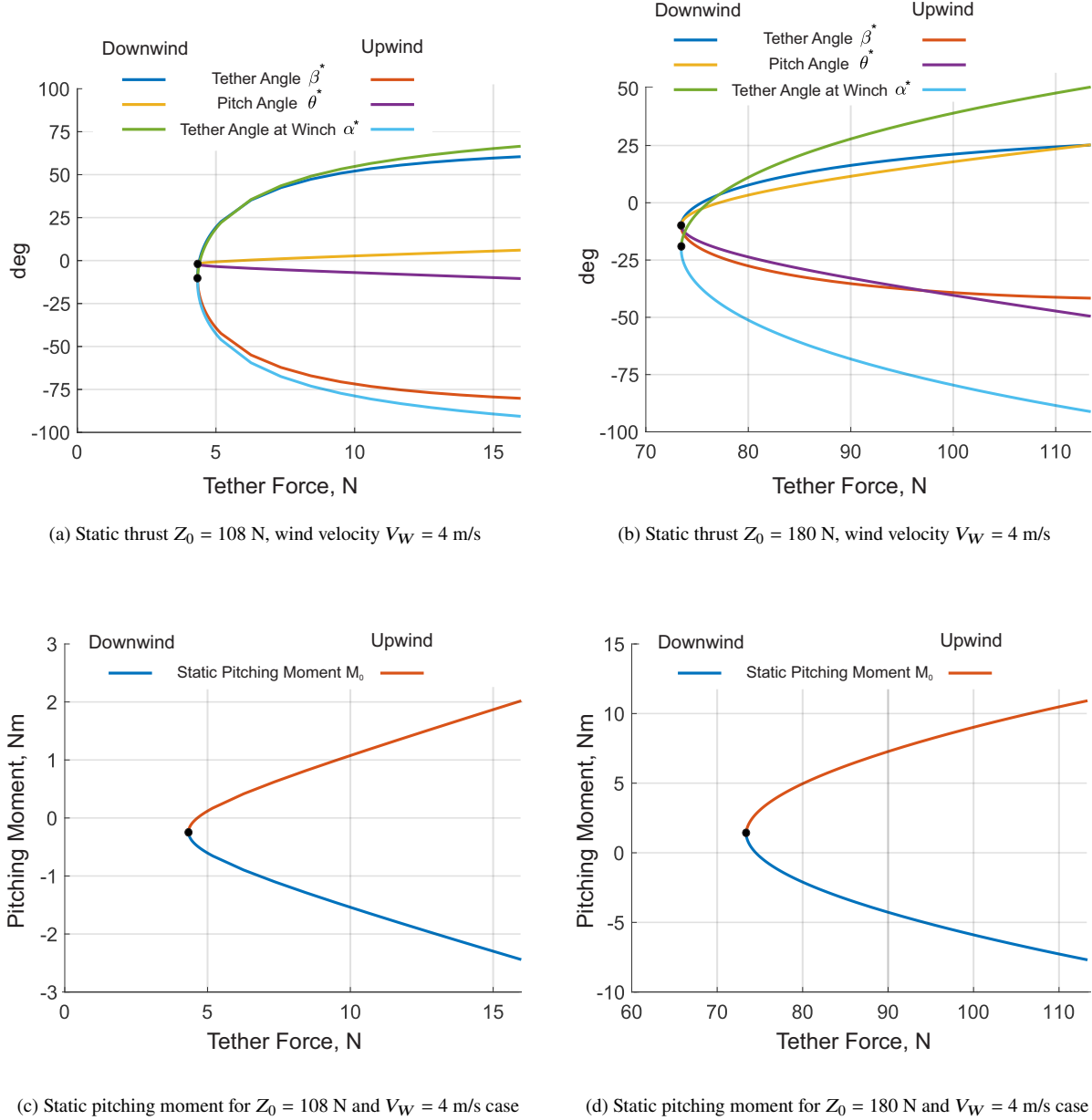(d) Static pitching moment for $Z_0 = 180$ N and $V_W = 4$ m/s case

**Fig. 3   Solutions for tether angles, pitch angle, and static pitch moment and under variation of tether force $T$. The dots mark points where only one solution is obtained. Otherwise, one upwind and one downwind solution exist.**

Both figures show a region to the left, in which the tether force is too low to produce an equilibrium of the system. This can be explained by the choice of static thrust $Z_0$, which overcompensates the weight of the vehicle and thus
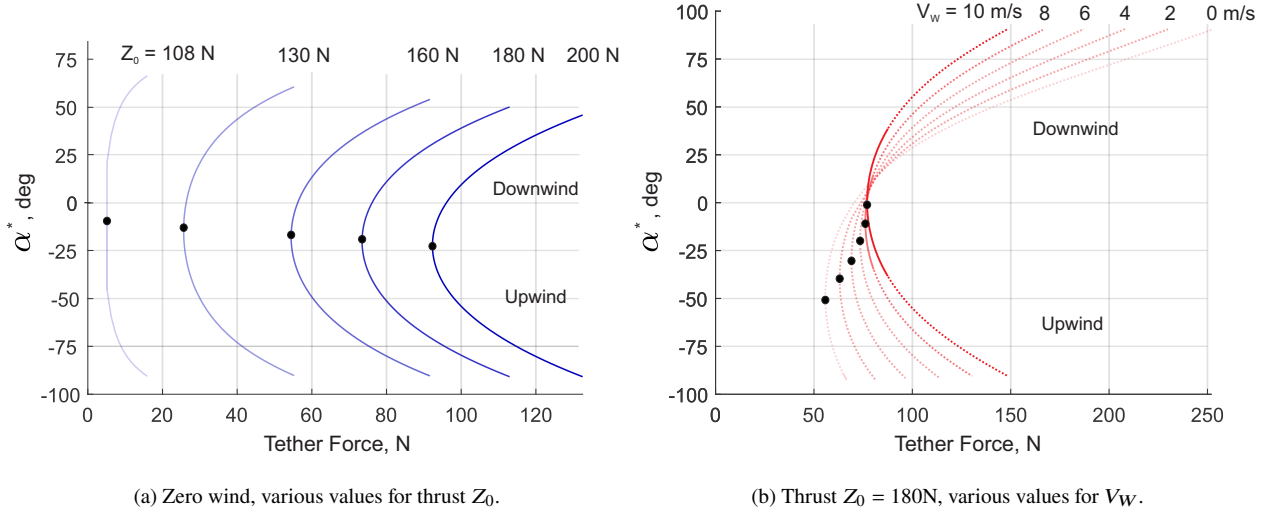
(a) Zero wind, various values for thrust $Z_0$.

(b) Thrust $Z_0 = 180$N, various values for $V_W$.

**Fig. 4 Solutions for $\alpha^*$ under variation of tether force $T$. The dots mark where upwind and downwind solution merge to a single solution.**

requires a certain tether force to counteract. Otherwise, the vehicle would start climbing.

Equations 34 and 35 produce exactly one solution when the tether force and weight of th helicopter exactly compensate $Z_0$. From this point on, increasing tether forces produce symmetrical solutions for $\alpha^*$, $\beta^*$, and $\theta^*$. One solution is upwind of the winch and one downwind of the winch. In the plots, we limited the maximum tether force to the point where the tether angle $\alpha$ exceeds 90°. An angle of 90° implies that the model hits the ship deck.

Figure 3 also shows that the position of the model (expressed by $\alpha^*$) and the pitching moment $M_0$ are sensitive to changes of tether force $T$ when the model is operated closely to the single solution point. The sensitivity decreases towards higher tether forces as $\alpha^*$ approaches 90°. The sensitivity to changes of $T$ can be decreased by choice of higher static thrust $Z_0$ (see Fig. 4a) and naturally changes with the horizontal wind $V_W$ as shown in Fig. 4b. Note that Fig. 4 uses dashed lines to indicate that the roots of the linearized system's vertical and short term pitching motion indicate damped oszillation. This is further discussed in Section IV.B.

Lowering the sensitivity of the position to changes of tether force $T$ may accomplish two things. First, the requirements for the winching device to produce and maintain a precise and steady force could be lowered, which would generally reduce system complexity and costs. Second, it simplifies the problem for the flight controller to adjust the trim to hold the position and/or attitude with respect to ship and winch.

Figure 4b shows the impact of wind on the sensitivity of $\alpha^*$ to changes of tether force $T$. The wind introduces additional drag forces which require the model to use some of the thrust $Z_0$ to counteract. In consequence, the minimally required tether force to establish equilibrium is lower and the solutions for $\alpha^*$ move to the left for increasing wind velocities.

The wind influence shifts the region of highest sensitivity of $\alpha^*$ to changes of $T$ towards negative values for $\alpha^*$, marked by the dots in Fig. 4b. This shift has two positive effects. Firstly, the position directly above the winch ($\alpha^* = 0$) becomes less sensitive to $T$ and the sensitivity decreases further for downwind positions. In downwind position, the model is pitching upward and behaves similarly to a kite. The benefits of operating tethered rotorcraft in the downwind domain is actually not new to aviation. Liptrot describes in [14] how early German approaches to use tethered rotorcraft as manned observation posts in the 1930s benefited from the increased stability of a downwind position.

An interesting finding of Fig. 4b is that the solutions for all wind velocities seem to intersect each other in a region

11

at $\alpha^* = 12°$ and $T = 81$ N. This region has the advantage that changes to the wind velocity have only little effect on the position whereas the thrust to force ratio is rather low.

The main results of our sensitivity analysis of the model's equilibrium points are as follows:
- High values for the static thrust $Z_0$ and according tether force $T$ reduce the sensitivity to changes of wind and tether force.
- A high horizontal wind velocity $V_W$ reduces the sensitivity to changes of tether force.
- Downwind positions of the rotorcraft to the winch are less sensitive to changes of wind and tether force than upwind positions.
- One region of downwind position and tether force is less sensitive to changes of wind velocity than the other regions.

**B. Eigenvalues of the Linearized Open-Loop Dynamics**

Linearization of the nonlinear system around an equilibrium $\mathbf{x}_P$ yields the linear dynamics of the longitudinal motion $\mathbf{A}_{lon}$. Figure 5a shows the roots of the linear dynamics for the model without tether influence and for variation of wind velocity. The roots for zero wind show the stable and oscillating phugoid for hover and one stable and one unstable root for pitching motion. At wind velocity of 13 m/s, the pitching motion stabilizes and with little more increase of wind velocity, the pitching motion begins to oscillate. The dot-dashed lines in Fig. 4 of the previous section indicate this oscillation. The solid lines mean, that vertical motion and pitching motion do not oscillate. At wind velocity of 17 m/s, the phugoid becomes unstable, while the frequency of oscillation continues to increase. Figure 5a shows also the roots for the position defined by tether length $L$ and tether angle $\beta$.

The most notable effect of the tether influence is depicted in Fig. 5b. Here, the equilibrium points are defined by a fixed thrust of $Z_0 = 130$ N, fixed tether force $T = 27$ N, tether length $L = 5$ m, while the wind velocity is varied. When compared with Fig. 5a, it becomes visible, that the poles of the model are much less sensitive to changes of the wind velocity. This advantage is very useful for controller design.

Figure 5c shows the change of roots for no wind and variation of tether force while the thrust $Z_0$ is held at 130 N and the tether length is 5 m. This diagram shows the dynamic stability of the system for the $Z_0 = 130$ N line in Fig. 4a. An increase of tether force leads to lower oscillation frequencies of the pitching motion, but increases the oscillation of the phugoid. Technically, the term phugoid is not valid since the tether influence alters the exchange of potential and kinetic energy, the defining principle of the phugoid. For simplicity, we will still use the term phugoid to refer to the tether influenced coupling of the translational vertical and horizontal motion.

Figure 5d displays the influence of the tether length on the dynamics. The diagram shows equilibrium points defined by a fixed thrust of $Z_0 = 130$ N, fixed tether force $T = 27$ N and $\beta^* = \theta^* = 0$ in zero wind. The motion pattern of the poles compares well to the results of Kaufman and Schultz [3]. Increasing tether length decreases the phugoid oscillation (pendulum mode), and increases the stability of the pitching motion (pitching mode). The phugoid poles shift slightly to the right.

# V. Conclusion

This paper introduces a simplified model of a tethered rotorcraft and presents the modeling approach to create this model. We use the model to identify equilibrium points and their sensitivity and stability under variations of tether force, tether length, wind velocity, and trim conditions. In fact, our results show that the tether creates two unstable equilibrium points, one downwind and one upwind, for a given ratio of thrust and tether force. Trivially, we cannot obtain equilibrium if the tether force is too low to compensate the thrust. The downwind and upwind equilibrium positions merge at a position defined by the lowest possible tether force to thrust ratio and the wind velocity. Around this point, the model's equilibria react most sensitively to changes of the tether force. However, higher thrust and tether forces generally robustify the equilibria to changes of tether force and also of wind velocity. The increase of robustness against wind is to be expected as high tether forces overshadow the drag forces. However, we found a region of rather small thrust to force ratio where a downwind position of the model appears to be robust to variations of the wind velocity.
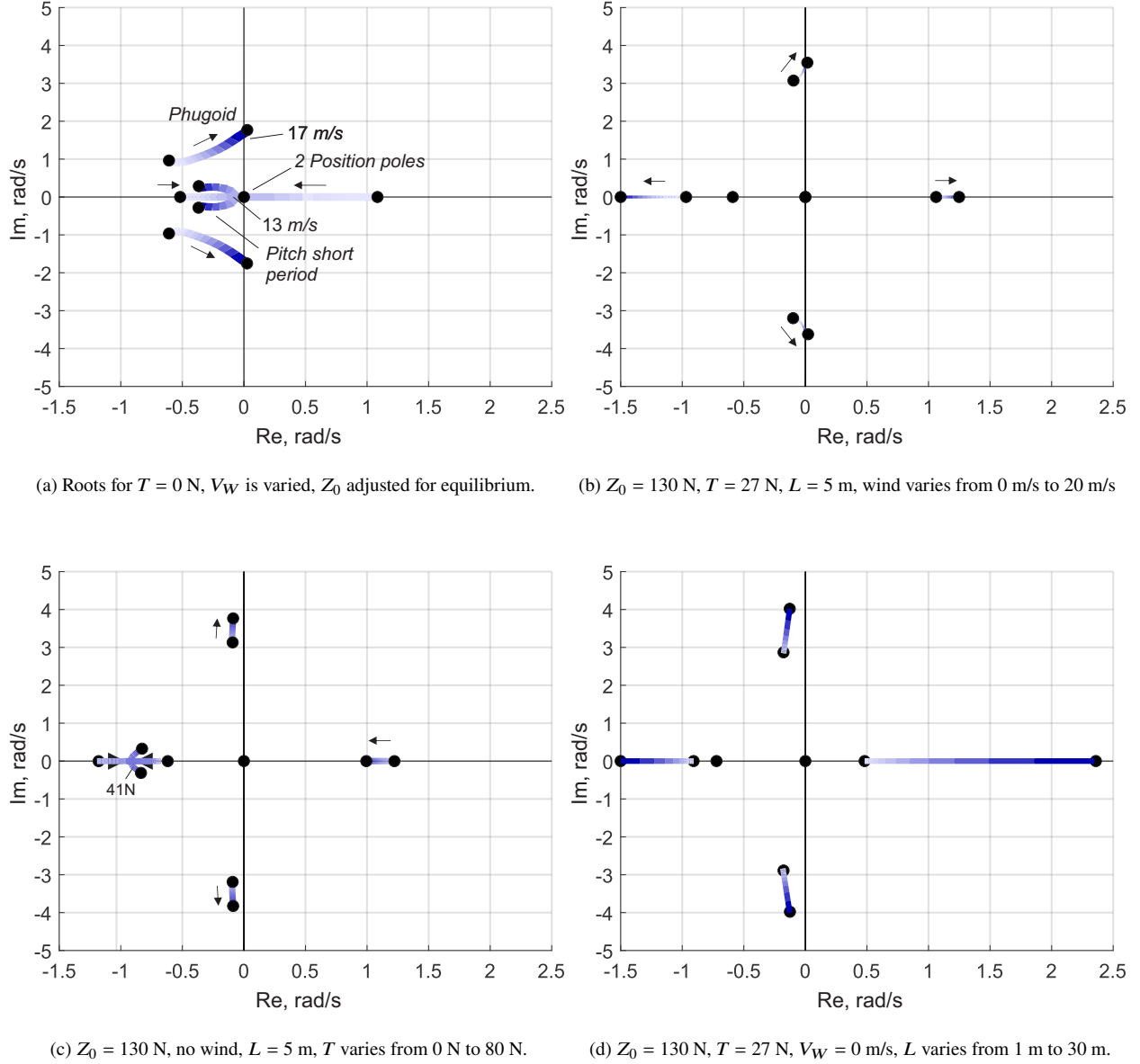
(a) Roots for $T = 0$ N, $V_W$ is varied, $Z_0$ adjusted for equilibrium.

(b) $Z_0 = 130$ N, $T = 27$ N, $L = 5$ m, wind varies from 0 m/s to 20 m/s

(c) $Z_0 = 130$ N, no wind, $L = 5$ m, $T$ varies from 0 N to 80 N.

(d) $Z_0 = 130$ N, $T = 27$ N, $V_W = 0$ m/s, $L$ varies from 1 m to 30 m.

**Fig. 5   Pole–zero plots for variations of different parameters. The color gradient goes from light blue (small parameter value) to dark blue (large parameter value).**

The analysis of the open-loop system's eigenvalues for the equilibrium points shows the impact of changes to tether force, tether length, and wind velocity on the model's stability. For the considered cases, the results show that the tether is not capable of changing the stability of the model. The unstable phugoid motion remains unstable, thus requiring the design of an appropriate controller to stabilize the model. However, we observed that increasing tether forces reduce the frequency of the unstable phugoid motion. Generally, our results indicate that a high tether force should be applied to the rotorcraft to create robustness of the position to changes of tether force and wind.

Ongoing work focuses on implementation of the model into a simulation environment to study the model's behavior to time-varying tether force and wind velocity. This would allow us to complement our current investigations of the static case. The simulation over longer periods of time requires stabilization of the model through the design and implementation of a suitable controller for the tethered system. Further steps are the improvement of the model, e.g.,

13

through integration of an accurate main rotor model, and parameter estimation based on experimental data. Model improvement and controller design are preliminary steps in preparation for subsequent experimental tests.

## Acknowledgments

## Appendix

**Table 1    List of model parameters.**

| Symbol | Name | Unit | Value |
|--------|------|------|-------|
| $m$ | Mass | kg | 10.5 |
| $g$ | Grav. Acceleration | m/s$^2$ | 9.81 |
| $I_{yy}$ | Moment of Inertia | kgm$^2$ | 0.5 |
| $\left[\mathbf{r}_{A/G}\right]_{\mathcal{B}}$ | Tether anchor offset | m | $[0, 0.15]^T$ |
| $\left[\mathbf{r}_{R/G}\right]_{\mathcal{B}}$ | Rotor forces offset | m | $[0, -0.12]^T$ |
| $\left[\mathbf{r}_{N/G}\right]_{\mathcal{B}}$ | Neutral point of aerodynamic forces | m | $[0.1, 0.1]^T$ |
| $X_u$ | Fuselage aerodynamic drag value in $x$ | kg/m | 0.028 |
| $X_{rd}$ | Horizontal rotor drag | s/m | -6e-3 |
| $Z_0$ | Static rotor thrust | N | 108 to 200 |
| $Z_{col}$ | Collective gain | N | 283.5 |
| $Z_{rd}$ | Vertical rotor drag derivative | s/m | 5e-2 |
| $Z_w$ | Fuselage aerodynamic drag value in $z$ | kg/m | 0.1108 |
| $M_{lon}$ | Pitch gain | Nm | -2.8 |
| $M_0$ | Static pitch moment | Nm | -15 to 15 |
| $T$ | Tether force | N | 0 – 100 |
| $V_W$ | Horizontal wind velocity | m/s | 0 to 15 |

## References

[1] S. Lorenz, and Chowdhary, G., "Non-Linear Model Identification for a Miniature Rotorcraft - Preliminary Results," *American Helicopter Society 61th Annual Forum*, Grapevine, Texas, USA, 2005.

[2] B. I. Schuchardt, T. Dautermann, A. Donkels, S. Krause, N. Peinecke, and G. Schwoch, "Maritime Operation of an Unmanned Rotorcraft with Tethered Ship Deck Landing System," *CEAS Aeronautical Journal*, 2020, pp. 1–9. https://doi.org/10.1007/s13272-020-00472-9.

[3] L. Kaufman, and E. R. Schultz, "The Stability and Control of Tethered Helicopters," *Journal of the American Helicopter Society*, Vol. 7, No. 4, 1962, pp. 41–54.

[4] S. Oh, K. Pathak, S.K. Agrawal, H. P., and M. Garratt, "Approaches for a Tether-Guided Landing of an Autonomous Helicopter," *IEEE Trans. Robot.*, Vol. 22, No. 3, 2006, pp. 536–544.

[5] B. Ahmed, and H. Pota, "Backstepping-based Landing Control of a RUAV Using Tether Incorporating Flapping Correction Dynamics," *Proceedings of the American Control Conference*, 2008, pp. 2728–2733.

[6] L. A. Sandino, M. Bejar, K. Kondak, and A. Ollero, "Advances in Modeling and Control of Tethered Unmanned Helicopters to Enhance Hovering Performance," *Journal of Intelligent and Robotic Systems*, Vol. 73, No. 1-4, 2014, pp. 3–18.

[7] L. A. Sandino, M. Bejar, K. Kondak, and A. Ollero, "Multi-Sensor Data Fusion for a Tethered Unmanned Helicopter Using a Square-Root Unscented Kalman Filter," *Unmanned Systems*, Vol. 4, No. 4, 2016, pp. 273–287.

[8] F. Alarcón, M. García, I. Maza, A. Viguria, and A. Ollero, "A Precise and GNSS-Free Landing System on Moving Platforms for Rotary-Wing UAVs," *Sensors*, Vol. 19, No. 4, 2019, p. 886.

[9] V. Gavrilets, B. Mettler, and E.Feron, "Nonlinear Model for a Small-Size Acrobatic Helicopter," AIAA Guidance, Navigation, and Control Conference and Exhibit, Montreal, Canada, 2001.

[10] F. Schettini, G. Di Rito, E.Denti, and R.Galatolo, "Nonlinear Model Identification of a Small-Scale Unmanned Rotorcraft," 30th Congress of the International Aeronautical Sciences, Daejeon, Korea, 2016.

[11] R. Cunha, and C. Silvestre, "Dynamic Modeling and Stability Analysis of Model-Scale Helicopters with Bell-Hiller Stabilizing Bar," AIAA Guidance, Navigation, and Control Conference and Exhibit, Austin, TX, USA, 2003.

[12] B. Mettler, M. B. Tischler, and T. Kanade, "System Identification of Small-size Unmanned Helicopter Dynamics," *Annual Forum Proceedings - American Helicopter Society*, Vol. 2, 1999, pp. 1706–1717.

[13] S. Sun, R. J. Schilder, and C.C. de Visserz, "Identification of Quadrotor Aerodynamic Model from High Speed Flight Data," 2018 AIAA Atmospheric Flight Mechanics Conference, Kissimmee, FL, USA, 2018.

[14] R.N. Liptrot, "Rotating Wing Activities in Germany During the Period 1939-1945," B.I.O.S. Overall Report No. 8. Published for the British Inteligence Objectives Sub-Committee by H.M. Stationery Office, London, United Kingdom, 1948.